NaOH Pretreated molybdate-carbon paste electrode for the determination of phosphate in seawater by square wave voltammetry with impedimetric evaluation

Mahmoud Fatehy Altahan[1,2z], Eric P. Achterberg[1] , Asmaa Galal Ali[3], Magdi AbdelAzzem[3]

[1] Chemical Oceanography Department, GEOMAR Helmholtz Center for Ocean Research Kiel, Kiel 24148, Germany.

[2] Central Laboratory for Environmental Quality Monitoring, National Water Research Center, El-Qanater El- Khairia 13621, Egypt.

[3]Electrochemistry Laboratory, Chemistry Department, Faculty of Science, Menoufia University, Shibin El-Kom 32511, Egypt.

[z]Email: maltahan@geomar.de; mahmoud_abdalqader@nwrc.gov.eg

DOI: 10.1149/1945-7111/ac3b03

Abstract

Phosphate (PO_4^{3-}) is an important nutrient for phytoplankton growth and at high loadings can result in water quality deteriorations. Autonomous PO_4^{3-} measurements are required for monitoring purposes, and are best achieved using sensitive, portable and lowcost techniques. Here we describe a new electrochemical sensor for PO_4^{3-} detection in seawater. The electrochemical quantification of PO_4^{3-} typically depends on the reaction between molybdate and PO_4^{3-} under acidic conditions to form a phosphomolybdic complex, which is electrochemically active. In this work, we prepared a carbon paste electrode (CPE) modified with molybdate and pretreated in 0.1 M NaOH using cyclic voltammetry (CV). The modified CPE was employed for the determination of PO_4^{3-} in artificial seawater (35 g/L NaCl) acidified with sulfuric acid to pH 0.8. The analytical conditions, including pH, waiting time for complexation, square wave amplitude and frequency, were optimized. An additional cleaning step (cyclic voltammetry (CV)) of 10 cycles in 0.1 M NaOH at −0.5 to 0.5 V was required between PO_4^{3-} determinations to dissolve the phosphomolybdic complex formed on the surface of the working electrode. Electrochemical impedance spectroscopy (EIS) results confirmed that the molybdate-modified CPE (molybdate/CPE) exhibited a low charge-transfer resistance (R_{ct}) toward PO_4^{3-}, and showed an improved analytical performance for different concentrations of PO_4^{3-}. A calibration plot in the range of 0.01–5 μM with a limit of detection (LOD) of 0.003 μM was obtained. The proposed electrode demonstrated good precision (4.3% and 5.8%) for concentrations of 5 and 0.2 μM, respectively. The proposed method was employed to analyze PO_4^{3-} in seawater samples on a research cruise in the North Sea, with results in close agreement to those obtained using conventional colorimetric measurements.

Keywords

Molybdate; Carbon paste electrode; Phosphate sensor; Electrochemical in-situ sensor; Seawater analysis

Introduction

Phosphate (PO_4^{3-}) is a key nutrient necessary for the growth of marine phytoplankton. Its availability determines the primary production and species composition of phytoplankton in coastal and oceanic waters. Surplus nutrient inputs, including phosphate, from anthropogenic sources lead to excessive algal growth and the subsequent depletion of oxygen caused by the remineralization of sinking dead algal biomass; this phenomenon is called eutrophication. Phytoplankton blooms may also cause the release of algal toxins that can have serious impacts on ecosystem and human health (1, 2). Therefore, monitoring the concentrations of PO_4^{3-} in marine waters is important to assess water quality (3). Generally, colorimetric techniques are used for the analysis of PO_4^{3-} in natural waters. The methods involve the complexation of PO_4^{3-} by molybdenum ions with the aid of antimony tartrate ($C_{12}H_{12}O_{18}Sb_2$) in the presence of a reducing agent to form the blue phosphomolybdate ($H_4PMo_8^{VI}Mo_4^{V}O_{40}$), which demonstrates a maximum absorbance at a wavelength of 880 nm (4). Alternatively, in the presence of vanadate ions, PO_4^{3-} can react with molybdate ions to form the yellow vanadomolybdophosphoric acid ($H_4PVMo_{11}O_{40}$), which is colorimetrically detected at a wavelength of 385 nm (5). Various wet chemical insitu monitoring instruments, including lab-on-a-chip sensors, have been developed based on the blue or yellow methods and deployed for PO_4^{3-} analysis in marine waters over periods up to several weeks (6, 7). However, these wet chemical techniques are limited by the consumption rate of reagents and instability of some reagents, e.g., ascorbic acid.

For field measurements, electrochemistry offers an excellent alternative to wet chemical approaches as it facilitates miniaturization, minimal power and reagent consumption, and reduced response times. For chemical oceanography, electrochemical devices have been developed for potentiometric pH monitoring (8), amperometric measurement of dissolved oxygen (DO) (9), trace metal speciation analysis using voltammetry(10-13), and conductivity/salinity measurements.

Several electroanalytical methods have been developed to detect PO_4^{3-}, and they offer a range of advantages. They do not require ascorbic acid as a reductant, and are fast and cost-effective, and do not require interventions related to turbidity interferences in the sample (14). In addition, using electroanalytical methods, it is possible to create a portable analyzer that could be used for field analysis of PO_4^{3-}. Over the last few decades, a number of electrochemical sensors have been reported that detect PO_4^{3-} in fresh or marine water by sensing phosphomolybdate complexes and utilizing cathodic reduction processes instead of a reductant.

The various electrochemical techniques for PO_4^{3-} analysis include amperometry, as reported by Udnan et al. (15). These workers used a glassy carbon electrode to detect PO_4^{3-} based on the reduction reaction with acidic molybdate, and applied flow injection amperometry for fresh and sea water samples. Amperometry was also utilized by Janca et al. (16), where self-production of molybdate ions inside the electrochemical cell was performed via the direct electrolysis of a molybdenum electrode. However, amperometry is complex because it requires the use of a rotating disk electrode, which makes it more complicated for field monitoring (17). Cyclic voltammetry has been utilized with a modified screen-printed electrode for the

quantification of PO_4^{3-} in mineral and river waters (18). Despite the simplicity and speed offered by cyclic voltammetry, the sensitivity is insufficient for the measurement of PO_4^{3-} in seawater, where the concentration ranges from a few nanomolar to 5 µM.

In contrast, pulsed techniques offer enhanced sensitivity and access to a wide range of time scales and background suppression options (19, 20). One of these techniques is differential pulse voltammetry (DPV), which was utilized in an autonomous, reagentless electrochemical method with a limit of detection (LOD) of 0.19 µM (17). However, it is difficult to optimize the parameters and achieve adequate repeatability with DPV.

Another pulsed technique, square wave voltammetry (SWV), combines the best aspects of several pulsed techniques and exhibits a better sensitivity than DPV (20). SWV was first utilized by Barus (21), who used a static gold electrode as working electrode with a molybdenum electrode to electrolytically generate molybdate with a LOD of 0.05 µM. The waiting time for complexation was 60 min, and an LOD value of 0.01 µM was achieved with a 30 min waiting time. Although the waiting time could be reduced to 5 min by separating the compartments for detection and complex formation, a LOD was not reported for the linear range.

Recently, several modified electrodes have been prepared for PO_4^{3-} analysis. Kumar et. al. (22) reported a wearable polyaniline/coconut shell carbon/poly(vinylidene fluorideco-hexafluoropropylene) sensor preloaded with ammonium heptamolybdate for the amperometric determination of PO_4^{3-} in river water samples. It showed a wide detection range (10-114 µM), but the LOD (0.6 µM) was not sufficiently low for analysis of natural waters. Wei et. al. (23) developed a modified screen printing electrode for DPV analysis of PO_4^{3-} in turbid coastal waters, with a linear detection range of 0.2 to 150 µM and a LOD of 0.05 µM.

A carbon paste electrode (CPE) was utilized for measuring PO_4^{3-} by Guanghan et al. (24), where a phosphomolybdic anion film was formed on the electrode surface using cyclic voltammetry in a solution containing PO_4^{3-} and molybdate. Then, the electrode was used to detect PO_4^{3-} via cyclic voltammetry with an LOD of 0.04 µg/mL (~0.4 µM). However, this study neglected the interference from silicic acid, which is the primary compound that interferes with PO_4^{3-} quantification in seawater using the molybdate chemistry.

The main challenge for utilizing electrochemistry for in-situ and real time determination of PO_4^{3-} is the lack of a direct and highly sensitive electrochemical sensor, which should be able to detect PO_4^{3-} in seawater, down to the nanomolar concentrations.

The aim of this work is to establish a rapid and sensitive electrochemical sensor for measuring PO_4^{3-} in seawater. For this, molybdate is added to a CPE to facilitate rapid formation of phosphomolybdate complexes, which can then be electrochemically detected using SWV or electrochemical impedance spectroscopy (EIS). The interference problems caused by silicic acid and a surfactant (Triton X-100) are investigated, and an application to natural seawater samples collected during a research cruise in the North Sea is presented. A comparison with the classical colorimetric method is also provided.

Experimental

Reagents and calibration standards

All the reagents were prepared using deionized (DI) water (resistivity >18.2 MΩ.cm, MilliQ, Millipore) and reagent grade salts. A thorough cleaning procedure was used to prepare all glassware and plasticware prior to use; they were rinsed with DI water and then soaked in a 10% HCl (v/v) (~1.2 M) bath (reagent grade, Carl Roth) for at least 24 h; finally, they were again rinsed with DI water. All of the calibration standards for PO_4^{3-} and silicic acid were prepared in artificial seawater with a salinity of 35, which was prepared using sodium chloride (NaCl, Merck) at 35 g/L. Stock solutions of 1 mM PO_4^{3-} (KH_2PO_4, Merck) and 1 mM silicic acid ($Na_2SiO_3.5H_2O$, Merck) were prepared by dissolving the salts in DI water.

Seawater sampling

Natural seawater samples were collected using rosette Niskin bottles on a CTD rosette frame (Multi water sampler SlimLine 6, Hydro-Bios, Germany) during a MOSES Stern 5 cruise in the North Sea (September 2020). The from was equipped with sensors for continuous acquisition of hydrographic data (Temperature, Salinity, pH, depth and dissolved oxygen). Seawater samples were filtered using a cartridge filter (0.2 µm pore size, Sartorius Sartobran P300) and collected in 50 mL polypropylene tubes for colorimetric nutrient measurements and 125 mL low-density polyethylene tubes for electrochemical measurements. The seawater samples were frozen at sea and analysed upon return to the land-based laboratory.

Colorimetric measurements

The colorimetric analysis of seawater samples was performed using a nutrient autoanalyzer (QuAAtro, SEAL Analytical) by applying the classical molybdenum blue method for PO_4^{3-} (7, 25, 26) and silicic acid (27), and applying the Griess reagent method for nitrite (NO_2^-) and with the assistance of a cadmium column (Seal Analytical) for nitrate (NO_3^-) (28). The baseline was established using artificial seawater that was prepared from NaCl. The detection limit was calculated as three times the standard deviation of the lowest concentration during the analytical run, which was 0.005 µM for PO_4^{3-}, 0.155 µM for H_4SiO_4, 0.028 µM for $\Sigma(NO_2^- + NO_3^-)$ and 0.004 µM for NO_2^-.

Apparatus

A potentiostat (µ-Autolab III, Metrohm, Netherlands) was employed for CV and SWV. A conventical three-electrode cell was utilized; it contained a working electrode (CPE, BASi, USA), a counter electrode (platinum wire, diameter 0.5 mm, Metrohm, Netherlands), and a reference electrode (Ag/AgCl, 3 M KCl, Metrohm, Netherlands). All potentials were reported against the reference electrode. EIS measurements were performed on a Model VersaSTAT 4 potentiostat (Princeton Applied Research, Oak Ridge, TN, USA), and all data were processed

using EC-Lab software (Bio-Logic, USA), which was also employed to fit and interpret the experimental results according to the equivalent circuit. Surface morphology analysis and elemental mapping of the molybdate/CPE were conducted using Field-emission scanning electron microscope (FE-SEM) (Gemini Ultra55 Plus, Zeiss, Germany) attached with an energy dispersive x-ray instrument (EDX) (X-act, Oxford Instruments, UK).

Preparation of the modified electrodes

The construction of the molybdate/CPE involved several steps. First, 0.7 g of graphite powder (particle size <20 μm, Sigma Aldrich, USA) was mixed with 0.3 g of paraffin oil (Sigma Aldrich, USA) in a mortar for 10 min to form a uniform carbon paste. Then, 0.1 g of ammonium molybdate tetrahydrate [$(NH_4)_6Mo_7O_{24}\cdot 4H_2O$] (≥ 99%, Sigma Aldrich, USA) was mixed with the resulting carbon paste (CP) in the mortar. The obtained mixture was pressed into the hole at the end of an electrode holder (BASi, USA) to prepare a modified molybdate/CPE. Subsequently, any excess electrode material was removed by polishing with a piece of filter paper (Whatman, England). The resulting modified CPE was rinsed with DI water and immersed in a solution of 0.1 M NaOH; then, CV was performed from −0.5 to 0.5 V for 10 scanning cycles at a scan rate of 0.1 V/s. Finally, the modified electrode was rinsed again with DI water, and then, it was used for measuring PO_4^{3-}.

Electrochemical measurements

Phosphate was measured using the modified electrode with SWV and a potential range of −0.2 to +0.8 V with a SW frequency of 150 Hz, a SW amplitude of 50 mV, and a step potential of 1 mV. All solutions were acidified using sulfuric acid (H_2SO_4, 98%, Merck) to reach a pH value of 0.8 prior to analysis. EIS measurements were performed from 0.25 Hz to 10 kHz for artificial seawater and from 0.1 Hz to 10 kHz only with the CP electrode.

Results and discussion

Electrochemical pretreatment of molybdate/CPE

The chemistry of molybdenum is complex because of its wide range of potential oxidation states (−2 to +5) and coordination numbers (0 to 8). The stability and behavior of the different valent compounds of molybdenum are pH-dependent (29). The electrochemical oxidation of molybdenum has been performed under various conditions (30-32). However, there are a limited number of studies on the electrochemical behaviour of molybdenum electrodes in a basic medium and our understanding of the products obtained under these conditions is still limited.

The molybdate/CPE underwent CV in a solution of 0.1 M NaOH, and repetitive scanning was used to assess the formation of MoO_4^{2-}. A possible formation pathway is indicated by the following equations:

$$Mo + 2\,OH^- \rightarrow Mo(OH)^{+}{}_2 + + 3e^- \quad (1) \quad (32, 33)$$

$$Mo(OH)^{+}{}_2 + 6\,OH^- \rightarrow MoO^2{}_4{}^- + 4\,H_2O + 3e^- \quad (2) \quad (32, 33)$$

After 10 consecutive CV sweeps in NaOH, the charge-transfer steps yielded the final Mo(VI) species MoO_4^{2-} on the working electrode surface. After this treatment with NaOH, the modified electrode was immersed in a solution of artificial seawater containing PO_4^{3-}, where the phosphomolybdate complex was formed under acidic conditions. After repeating the same procedure in 0.1 M H_2SO_4, the molybdate/CPE did not indicate any clear voltammetric peaks, even over 1 μM PO_4^{3-} concentrations in the solution.

SWV of PO_4^{3-}

Phosphate cannot be detected directly because it is an electrochemically inactive species. However, it can be electrochemically interrogated in a highly acidic medium in the presence of molybdate ions, where it can form a phosphomolybdate complex, which is also known as the Keggin ion (Equation 3).

$$7H_2PO_4 + 12\,MoO^2{}_4{}^- + 72H^+ \rightarrow 7[PMo_{12}{}^{(VI)}O_{40}]^{3-} + 36H_2O \quad (3) \quad (34)$$

This approach suffers from cross interference from silicic acid, which has the same affinity for molybdate to form a silicomolybdate complex. The interference can be reduced by altering the ratio of H^+ to MoO_4^{2-} to between 60 and 80, and adjusting the pH to between 0.4 and 0.9 (17, 35). In the current study, the pH of the electrolyte medium was adjusted using sulfuric acid to pH 0.8. Under these conditions, SWV was performed from −0.2 to 0.8 V. **Figure 1** shows the SWVs of 0.5 μM PO_4^{3-} in artificial seawater in acidic conditions at the molybdate/CPE before and after the treatment with NaOH. Without the NaOH pretreatment, five oxidation peaks at −0.12 V, 0.03 V, 0.1 V, 0.28 V, and 0.5 V (peaks I to V, respectively) were observed, which are likely related to the formation of different phosphomolybdate polymeric structures generated by the coupling between molybdate ions and PO_4^{3-}(36, 37). At various PO_4^{3-} concentrations, the relationship between the peak current for all the various peaks and the PO_4^{3-} concentration was not linear which was likely caused by the adsorption of phosphomolybdate polymers onto the working electrode surface (38). In contrast, the molybdate/CPE that had been pre-treated with consecutive CVs in NaOH showed a different electrochemical behaviour toward PO_4^{3-} ions. The voltammograms show two oxidation peaks at 0.21 V and 0.58 V, corresponding to peak I and II, respectively. These two peaks are related to the electrooxidation of Mo(II) to Mo(IV) and Mo(IV) to Mo(VI), respectively (39). The current of the peak at 0.21 V increases with increasing concentration of PO_4^{3-}, demonstrating a good electrochemical behaviour.

Figure 1

Surface morphology and X-ray analysis

The structure and surface morphology of the molybdate/CPE before and after pretreatment by CV in 0.1 M NaOH, and after SWV in a solution of artificial seawater (pH 0.8) containing 1 µM PO_4^{3-}, were studied using FE-SEM as shown in **Figure 2**. The components present on the surface were also confirmed by EDX spectra and show the distribution of the components in the studied region by elemental mapping analysis (**Figure 2), (Figure S1**). Figure 2, A shows an image of molybdate/CPE at low magnification (100 µm), where the carbon paste can be seen as a pattern of irregular sheets, while molybdate oxide can be seen on the image at high magnification (20 µm) as a white spot surrounded by a dark graphite network. The selected spot contains about 95.7% carbon, 3.42% oxygen and 0.85% molybdenum. Figure 2, B shows the increase in thickness of the molybdate oxide structure, which appears as a dense white spot after modification by CV in 0.1 M NaOH. The EDX showed the increase in molybdate oxide with about 1.51% molybdenum, 8.51% oxygen and 89.9% carbon. This explains the improvement in the electrochemical sensor performance by the pretreatment step in NaOH solution. After SWV in a solution of 35 g/L (pH 0.8) containing 1 µM PO_4^{3-}, the molybdate/CPE exhibited a thick white spot of molybdenum oxide in which PO_4^{3-} was present, as shown in **Figure 2, C**, which was indicated by the mapping analysis where phosphorus appeared as orange dots in the spot of molybdenum oxide (**Figure S1J**). This indicates the formation of a Keggin-type phosphomolybdate complex on the molybdate/CPE pretreated with NaOH. However, the phosphorus content cannot be seen in the EDX spectra because the phosphorus concentration was extremely low compared to other components (C, Mo, O) physically embedded in the paste, while PO_4^{3-} comes from a solution of 1 µM.

Figure 2

Optimization of analytical conditions

The analytical method was optimized by investigating the influence on the signal of different analytical conditions, including pH of the medium, quiet time before measurement, and square wave parameters, including frequency and amplitude.

The sensitivity of the electrochemical measurement of PO_4^{3-} based on the molybdate method is strongly affected by pH. In addition, the selectivity of the method is influenced by the acid concentration as an optimized pH value is essential to exclude the interference by silicic acid, which is present in seawater at concentrations ranging from ~0.5 to 200 µM. To illustrate the pH dependency, the peak current of 0.01 µM PO_4^{3-} in artificial seawater at the molybdate/CPE was recorded in the pH range from 4.6 to 0.3 (**Figure S1A)**. It was observed that when the pH decreased, the peak current increased, reaching a maximum peak current of 4.4 µA at pH 0.8 and pH 0.6. To minimise the amount of sulfuric acid needed to acidify the sample prior to the analysis, pH 0.8 was chosen as the optimal pH value.

The quiet time is the period between the insertion of the working electrode into the electrolyte and the commencement of the potential scan. After transferring the electrodes from a very basic medium (0.1 M NaOH, pH ~12.6) to a highly acidic medium (pH 0.8), setting a quiet time before generating phosphomolybdate complexes during the PO_4^3measurement allows for adequate mixing of PO_4^{3-} ions with molybdate ions on the working electrode surface. The quiet

time was varied from 0 to 300 seconds and the resulting voltammetric behaviour was recorded for 0.01 μM PO_4^{3-} in artificial seawater (pH 0.8) **(Figure S2B**). Increased peak currents were observed when the quiet time was increased from 0 s (0.3 μA) to 90 s (2.2 μA). This behavior is likely caused by an increased amount of PO_4^{3-} ions adsorbed on the surface of the molybdate/CPE after prolonging the quiet time. At longer quiet times, no further enhancement was observed, probably due to saturation of the working electrode surface with adsorbed PO_4^{3-} ions before analysis. Thus, 90 s of quiet time was found to be suitable for the PO_4^{3-} determination.

A square-shaped potential pulse is employed in SWV that is produced periodically with a staircase potential ramp. In addition, SWV combines three components that can be optimized to increase the sensitivity and performance of the method. The components include the staircase potential modulation or step potential (E_{step}) and the height of the potential pulse or square wave amplitude, which is larger than the step potential (both are measured in mV). The period of one potential cycle is described by its reciprocal or frequency (f) in Hertz (Hz). Here, the effect of varying two square wave components (amplitude and frequency) on the peak current values at a constant step potential value (1 mV) was studied. The influence of the square wave amplitude on the peak current of 0.01 μM PO_4^{3-} was evaluated from 10 to 100 mV (**Figure S2C**), and it was observed that the peak current increased at higher square wave amplitudes up to 50 mV to generate a maximum value of 2.05 μA. At amplitudes higher than 50 mV, the peak currents decreased to 1.8 μA and 1.6 μA for 75 mV and 100 mV, respectively. Thus, 50 mV was determined to be the optimal square wave amplitude, where higher values resulting in a slight decrease of the peak current. The scan rate (ν) for SWV is assigned in terms of the step potential and frequency ($\nu = E_{step} \times f$)/mVs^{-1}. To study the influence of the square waveform scan rate on the peak current, the frequency was varied from 10 to 200 Hz (**Figure S2D**) while holding the step potential constant at 1 mV to reduce the peak noise (at higher than 1 mV, a distortion of the peak voltammogram was observed). The peak current was found to increase linearly with frequency until 150 Hz. Therefore, the optimum frequency, i.e., the scan rate, was approximately 150 Hz with a related peak current value of 4.5 μA, and at higher scan rates, the peak current decreased slightly to 4 μA at a frequency of 200 Hz.

Impedimetric performance

Electrochemical impedance spectroscopy was used to analyze the properties of the analytical method by accounting for the possible positions of all components in the electrochemical cell (resistors, conductors, capacitors) and their influences on the movement of ions and electrons by applying alternating current signals and recording the response as a function of frequency. The resulting electrical output signals were sinusoidal at different times (phase-shifted) as a function of the voltage. EIS can be evaluated using two approaches: Nyquist plot and Bode plot. The Nyquist plot compares the imaginary impedance component (out-of-phase, Z_{Im}) against the real impedance (in-phase, Z_{Re}) at each applied frequency. The Bode plot compares the logarithm of the absolute impedance |Z| and the phase-shift against the logarithm of the applied frequency (40). To test the impedimetric responses of the bare electrode, CPE,

and molybdate/CPE, EIS was performed in a solution containing 0.1 μM PO_4^{3-} in artificial seawater at a pH of 0.8 at both electrodes.

The Nyquist and Bode plots are shown in **Figure S3 (A, B)**, and a modified Randles equivalent circuit was used to fit the experimental data (**Figure S3C**). The data fit using this circuit are represented by solid lines in the EIS spectra. A good match was observed between the experimental and fitted data. The equivalent circuit used to model the data is associated with the resistive and capacitive components. The components of the circuit are as follows: solution resistance R_s, double layer capacitance Y_o1, capacitance of the film Y_o2, chargetransfer resistance R_{ct}, film resistance R_f, and Warburg impedance W_s1. All of the fitting data are listed in **Table S1**. The suitability of the model circuit is indicated by the sum of the weighted error, or X^2, where a smaller value of X^2 indicates a good fit of the experimental data (41). It was found that for the CPE and molybdate/CPE, the variation in the value of R_s was not high because the values of R_s only depend on the ionic strength of the electrolyte solution and the distance between the auxiliary and working electrodes in the electrochemical cell (42), and the ionic strength of the electrolyte solution remained constant (0.1 μM PO_4^{3-} in artificial seawater at pH 0.8). Y_o1 is the double layer capacitance on the interface between the electrode and its surrounding electrolyte. The double layer is formed as ions in the solution are deposited on the electrode surface. This value depends on many variables (e.g., electrode potential, ionic concentration, electrode roughness). The deviation of Y_o1 from perfect capacitance (n = 1) is due to the relatively small value of its components for both cases (n = 0.9287 for CPE) and (n = 0.8234 for molybdate/CPE). The relatively high value of n for molybdate/CPE indicates the capacitive nature of the proposed sensor toward PO_4^{3-}. The Y_o2 and W_s1 values generally relate to the diffusion of ions from the electrolyte solution to the surface of the electrode. The low values for both variables in molybdate/CPE as compared to CPE indicate that the proposed sensor is more diffusive for PO_4^{3-} than CPE. Among these variables, R_{ct} is the most essential element because it is related to the kinetics of the charge-transfer reaction at the interface. The measured values of $1.838 \times 10^6\ \Omega$ for CPE and 1.173 Ω for molybdate/CPE indicate fast kinetics of electrons in the presence of PO_4^{3-} at the modified electrode, while the decrease in R_f indicates lower resistance of the electrode film layer toward PO_4^{3-}.

Following analysis of the equivalent circuit and comparison of the influence of CPE and molybdate/CPE on the impedimetric signal of the electrolyte containing PO_4^{3-}, the response of the sensor to the presence of PO_4^{3-} in various electrolyte solutions was assessed. EIS was performed on molybdate/CPE for different concentrations of PO_4^{3-} in artificial seawater to evaluate its analytical performance. A series of EIS experiments were performed where the molybdate/CPE was exposed to increasing concentrations of PO_4^{3-}. The experimental data for the determination of PO_4^{3-} are represented by the corresponding Nyquist plot shown in **Figure 3A**. The data were fitted according to the modified Randles equivalent circuit presented in **Figure 3B** with the same components used in the equivalent circuit in **Figure S2**, with the exception of a constant phase element that was used rather than a capacitor for the film capacitance. The data in Figure 3C indicate a gradual decrease in the impedimetric signal in terms of the R_{ct} value, which is likely due to the release of electrons during the reaction of PO_4^{3-} ions with molybdate ions as part of the complexation process. The proposed sensor exhibited a

linear relationship between R_{ct} value and PO_4^{3-} concentration in the range of 0.1 to 1 μM with a sensitivity of −431.35 Ω.μM^{-1} and a coefficient of detection (R^2) of 0.982.

Figure 3

Analytical performance

Square wave voltammetry was employed for the quantitative measurement of PO_4^{3-} in artificial seawater (35 g/L NaCl) under acidic conditions (pH 0.8), including a washing step using CV for 10 cycles in NaOH between the measurements. The square wave voltammograms were recorded under the optimized conditions using a range of PO_4^{3-} concentrations (0.01, 0.02, 0.05, 0.1, 0.2, 0.4, 1, 2, 3, and 5 μM) (**Figure 4**). The data demonstrate a fairly linear relationship between the PO_4^{3-} concentration and peak current values at the molybdate/CPE. Two regimes of linear behavior were observed. The first was over a concentration range of 0.01 to 0.4 μM PO_4^{3-} with a slope of 13.9704 μA.μM^{-1} (R^2 = 0.99039), and the second linear regime was over a concentration range from 1 to 5 μM PO_4^{3-} with a slope of 0.3025 μA.μM^{-1} (R^2 = 0.9904). The separation of the data into two discrete linear ranges reflects the adsorption of the phosphomolybdate complex onto the electrode surface at high concentrations of PO_4^{3-}, similar to the behavior reported previously for electrochemical PO_4^{3-} sensors (21, 39, 43). This behavior was attributed to the formation of a polymer film of the phosphomolybdate complex at high concentrations of PO_4^{3-} (38, 44, 45), where the polymer film may act as an insulator to impede the electron transfer through the electrode surface. The LOD was calculated to be 0.003 μM based on the IUPAC recommendation (46) defined as three times the standard deviation of the analysis of blank solutions (n = 20), divided by the slope of the linear fit (slope of the calibration curve 0.01– 0.4 μM PO_4^{3-}).

Figure 4

Table 1 Summary of comparison of the molybdate/CPE modified electrode with those reported previously in the literature (18, 21, 39, 47-53). The proposed sensor was found to have a higher sensitivity, with only a screen-printed electrode reported by Kolliopoulos et al. in 2015 demonstrated a similar LOD for the quantification of PO_4^{3-} after complexation with molybdate in solution.

Table 1. Electrochemical determination of PO_4^{3-} using different working electrodes.

Electrode	**Technique**	**Linear range (μM)**	**LoD (μM)**	**Reference**
PANI	Amperometric	1-100	1	(47)
Bis(DBPS)methane/PVC	Potentiometric	0.5-5 × 10^3	0.5	(48)
Chitosan-clay/PVC	Potentiometric	1- 1× 10^4	0.6	(49)
Cu-BPMP	Potentiometric	3-50	0.5	(50)
CBNPs-SPE	Amperometric	1-80	0.1	(51)
CB/SPE	Amperometric	0.5-100	0.4	(18)
AuNWs	Amperometric	12.5-1 × 10^3	0.1	(52)

AuNWs/Pt	Amperometric	48-1.4 × 10^3	45	(53)
SPE	CV (Ammonium Molybdate tetra hydrate)	0.005- 0.2	0.003	(39)
Au electrode	SWV (Electrolytic produced Molybdate + NaCl)	0.1-1	0.05	(21)
Molybdate / CPE	SWV	0.01 - 5	0.003	This work

PANI = polyaniline, DBPS = Bis(dibromophenylstannyl)methane, PVC = polyvinyl chloride, BPMP = 2,6-bis(bis(2- pyridylmethyl)aminomethyl)-4-methylphenol, CB = carbon black nanoparticles, SPE = screen printed electrode, AuNWs = Gold-nanowires array

Reproducibility and stability of the modified electrode

The fabricated molybdate /CPE exhibited excellent repeatability (**Figure 5)** for SWV responses toward 0.2 and 5 μM PO_4^{3-}. The electrode was tested via 10 repetitive measurements of PO_4^{3-} employing the same sensor in the same solution, and the precision was determined by the relative standard deviation (RSD). For 0.2 μM PO_4^{3-}, an RSD value of 5.76% was obtained, and for 5 μM PO_4^{3-}, an RSD value of 4.32% was measured. The reproducibility of the sensor electrode was tested using five different sets of electrochemically fabricated electrodes, which generated an RSD value of 5.46% for 5 μM PO_4^{3-} and exhibited a good reproducibility with an independently fabricated electrode. The stability of the electrode was evaluated using the SWV responses recorded over five days (the modified electrode was stored at room temperature between uses), and an RSD value of 7.26% was obtained, possibly caused by the decrease of the signal over time, which may be improved by adapting the storage conditions. Overall, the electrochemically-modified electrode demonstrates good stability, reproducibility, and reparability characteristics for PO_4^{3-} analysis.

Figure 5

Interferences on PO_4^{3-} analysis

A surfactant is identified as a molecule containing both a hydrophobic head and end. Because of their unique chemical structure, surfactants affect the electrochemical process of substances by modifying the electrode-solution interface properties (54). Triton X-100 is a highly hydrophobic nonionic surfactant with an average of 95 ethoxy groups. In this study, Triton X-100 was selected because of its outstanding tendency to be adsorbed on the working electrode surface (55). The potential interference from Triton X-100 was assessed by varying the surfactant concentration in a solution of artificial seawater that was spiked with 0.01 μM PO_4^{3-} (**Figure 6A**). The addition of 1 mg/L Triton X-100 resulted in a decrease of the peak current compared to the 0.01 μM PO_4^{3-} standard solution, and a PO_4^{3-} underestimation of ~9%. For a solution containing 2 mg/L Triton X-100, the peak current decrease resulted in a PO_4^{3-} underestimation of ~7%. At 3 mg/L Triton X-100, the peak current was similar to a surfactant-

free solution, but beyond 3 mg/L the peak current increased until 8 mg/L resulting in a PO_4^{3-} overestimation of ~14%. At concentrations higher than 8 mg/L, a stronger interference was observed with an overestimation of ~40% and ~55% for 9 mg/L and 10 mg/L Triton X-100, respectively. The level of nonionic surfactants in natural waters is typically between 0.1 and 0.5 mg/L (56). Although there was an interference effect on the peak current measurement of PO_4^{3-} due to Triton X-100, the linearity of the response was not influenced, as shown in **Figure 6B**, where a calibration curve was established over the linear range of 0.01–0.05 μM PO_4^{3-} in a solution spiked with 10 mg/L Triton, with the regression equation, I_p (μA) = 24.9586 [PO_4^{3-}] (μM) + 0.84751 and an R^2 value of 0.994.

There is an interference in seawater by silicic acid on the determination of PO_4^{3-} Silicic acid competes with PO_4^{3-} to react with molybdate ions because of their similar ionic structure. To overcome this problem, the concentration of molybdate ions and protons (H^+) should be regulated in order to obtain an appropriate H^+ to MoO_4^{2-} ratio. Zhang et al. (57) demonstrated that it is possible to avoid the interference from silicic acid by conducting the analysis at a pH between 0.4 and 0.9 . We verified this assumption by testing various loading concentrations of silicic acid from 10 to 50 μM were tested at a constant concentration of PO_4^{3-} (0.05 μM) in a solution of artificial seawater (pH 0.8) (**Figure 6C**). The peak current of the standard PO_4^{3-} solution with and without silicic acid was measured after each addition, and the signal change did not exceed 7% with an increase of the silicic acid concentrations up to 50 μM, indicating the capability of the proposed method to exclude silicic acid interferent during real seawater analysis. The peak intensities are reported on the calibration curve between 0.01 and 0.2 μM PO_4^{3-} (**Figure 6D**, red dots), and the results demonstrate that silicic acid does not interfere in the PO_4^{3-} concentration determination.

Figure 6

Analysis of coastal seawater samples

As a demonstration of the proposed method to natural samples, discrete samples were collected at different stations in the North Sea between the coast and Helgoland Island (**Figure 7).** The research was conducted in the German Bight in the outflow plume of the Elbe River. The North Sea is a shallow, semi-enclosed shelf sea of the North Atlantic (58). In the North Sea, two water bodies can be distinguished. The northern and central parts are under oceanic influence with surface salinities under 34. The southern part is well mixed and receives oceanic water from the British Channel (58). In the coastal water, salinity is lower at 30 because of strong riverine influences (59). The Elbe River is one of the larger rivers discharging into the North Sea, with a length of 1.094×10^3 km and a catchment area of 148.268×10^3 km^2, categorized as the fourth largest catchment area of Central Europe
(60). The Elbe River is subject to high anthropogenic influences, and it represents the most frequent shipping route to Hamburg (50,000 vessels move through the river yearly). The Elbe River is considered one of the most heavily polluted rivers in Europe with low dissolved oxygen levels, organic matter enrichment, nutrient enrichment because of human activities, and navigation channel deepening (61, 62). (61, 63). The German Bight in the eastern North Sea receives oceanic water from the British Channel and the northwestern North Sea (64), with PO_4^{3-} concentrations of approximately 1.8 μM reported in September 2008 (65). The salinity

ranges from below 30 in front of Elbe outlets to 31–32 approximately 30 km from the coast. At 50 km offshore at Helgoland Island, salinity varies between 31 and 32, whereas at 75 km offshore, salinity is higher than 33 (66, 67). Figure 7 shows the spatial distribution of salinity gathered during CTD casts. The results revealed a complex dispersal of lower salinity inputs into the North Sea from the Elbe River. Salinity ranged from 27.3 to 33, with the lowest salinity close to the Elbe Estuary and all over the periphery of the North Sea and higher salinity toward the center.

Figure 7

The PO_4^{3-} concentrations in the collected samples were analyzed upon returning to the landbased laboratory using an electrochemical approach, discussed herein. A comparison with the classical colorimetric method was made for validation purposes. Figures 8A and B show that the PO_4^{3-} concentrations obtained using the colorimetric and electrochemical approaches, respectively, against the variation of the salinity data gathered during CTD casts. Both methods show significant negative correlations ($p < 0.01$) with salinity. Although the electrochemical approach showed a weaker correlation ($R^2 = 0.4$) compared with the colorimetric method ($R^2 = 0.78$), significant differences exist between them at the 1% significance level (paired *t*-test, $df = 23$), with $p = 6.59 \times 10^{-29}$ for those obtained electrochemically and $p = 7.9 \times 10^{-29}$ for those obtained using the colorimetric method. Considering all data, a mean accuracy of 93% (assessed as the average of the recovery values) for electrochemical measurements compared to the colorimetric data was obtained, exhibiting a strong significant correlation with the Spearman correlation coefficient of 0.75 ($p < 0.01$, $n = 23$) (**Figure 8C & Figure 9**). The PO_4^{3-} concentrations determined using the colorimetric method were between 0.687 and 1.769 µM, with a mean PO_4^{3-} concentration of 1.189 ± 0.273 µM ($n = 23$). The proposed electrochemical method obtained minimum and maximum PO_4^{3-} concentrations of 0.624 µM and 1.83 µM, respectively, with a mean of 1.195 ± 0.367 µM ($n = 24$). Both methods showed no significant differences in the analytical results at 1 % significance level with (*t*-test, *p*-value = 0.74, $df = 23$).

Figure 8

A Spearman correlation matrix (**Figure 9**) shows the relationships between the electrochemical determined PO_4^{3-} concentrations and other parameters determined in the discrete samples. For example, PO_4^{3-} concentrations significantly correlated with $\Sigma(NO_2^- + NO_3^-)$ and NO_3^- with positive correlation coefficients of 0.36 and 0.29; thus, the results show the relationship between the two main nutrients (N and P) required for primary production. The weak positive correlation with oxygen could refer to the enhanced PO_4^{3-} level due to riverine input and this could not be related to the biological activity. There is an anti-correlation with salinity, with a Spearman correlation coefficient of −0.629, which is related to the enhanced PO_4^{3-} concentrations from the freshwater Elbe river end-member.

Figure 9

Conclusion

In summary, a novel molybdate/CPE working electrode was presented for PO_4^{3-} sensing in seawater, which utilizes the formation of a phosphomolybdate complex to achieve high sensitivity and selectivity for PO_4^{3-} under acidic conditions. molybdate/CPE exhibited a wide detection range (0.01–3 μM) and a low detection limit of 0.003 μM at an RSD of 5.7% (for 0.2 μM, n = 10). In addition to the stability and reproducibility of the electrode, the sensor exhibited no interference from silicic acid, which is the most common interfering ion for PO_4^{3-} analysis in seawater. The proposed electrode was successfully utilized for real sample analysis and performed well as compared to the conventional colorimetric methods This study reveals the significant potential of the designed electrode to integrated into a portable electrochemical device for field testing PO_4^{3-} concentrations in marine waters.

Acknowledgments

All authors would like thank Prof. Dr. Amr Beltagi as he facilitated the EIS measurements on the VersaSTAT 4 Potentiostat in his laboratory at the Chemistry Department, Faculty of Science, Kafr El-Sheikh University, Egypt. M.F. Altahan wishes to thank the National Water Research Center (NWRC).

References

1. M. Salomon and T. Markus, *Handbook on Marine Environment Protection*, Springer (2018).
2. S. B. Bricker, B. Longstaff, W. Dennison, A. Jones, K. Boicourt, C. Wicks and J. Woerner, *Harmful Algae*, **8**, 21 (2008).
3. D. M. Karl, *Annual review of marine science*, **6**, 279 (2014).
4. E. A. Nagul, I. D. McKelvie, P. Worsfold and S. D. Kolev, *Analytica chimica acta*, **890**, 60 (2015).
5. C. Warwick, A. Guerreiro and A. Soares, *Biosens Bioelectron*, **41**, 1 (2013).
6. M. M. Grand, G. S. Clinton-Bailey, A. D. Beaton, A. M. Schaap, T. H. Johengen, M. N. Tamburri, D. P. Connelly, M. C. Mowlem and E. P. Achterberg, *Frontiers in Marine Science*, **4** (2017).
7. F. E. Legiret, V. J. Sieben, E. M. Woodward, S. K. Abi Kaed Bey, M. C. Mowlem, D. P. Connelly and E. P. Achterberg, *Talanta*, **116**, 382 (2013).
8. K. McLaughlin, A. Dickson, S. B. Weisberg, K. Coale, V. Elrod, C. Hunter, K. S. Johnson, S. Kram, R. Kudela and T. Martz, *Regional Studies in Marine Science*, **12**, 11 (2017).

9. N. P. Revsbech, L. H. Larsen, J. Gundersen, T. Dalsgaard, O. Ulloa and B. Thamdrup, *Limnology and Oceanography: Methods*, **7**, 371 (2009).
10. K. A. Howell, E. P. Achterberg, C. B. Braungardt, A. D. Tappin, D. R. Turner and P. J. Worsfold, *Analyst*, **128**, 734 (2003).
11. C. B. Braungardt, E. P. Achterberg, B. Axelsson, J. Buffle, F. Graziottin, K. A. Howell, S. Illuminati, G. Scarponi, A. D. Tappin and M.-L. Tercier-Waeber, *Marine Chemistry*, **114**, 47 (2009).
12. E. P. Achterberg and C. Braungardt, *Analytica chimica acta*, **400**, 381 (1999).
13. S. Illuminati, A. Annibaldi, C. Truzzi, M.-L. Tercier-Waeber, S. Nöel, C. B. Braungardt, E. P. Achterberg, K. A. Howell, D. Turner and M. Marini, *Marine Chemistry*, **212**, 47 (2019).
14. S. Berchmans, T. B. Issa and P. Singh, *Anal Chim Acta*, **729**, 7 (2012).
15. Y. Udnan, I. D. McKelvie, M. R. Grace, J. Jakmunee and K. Grudpan, *Talanta*, **66**, 461 (2005).
16. J. Jońca, V. León Fernández, D. Thouron, A. Paulmier, M. Graco and V. Garçon, *Talanta*, **87**, 161 (2011).
17. J. Jońca, M. Comtat and V. Garçon, **4**, 25 (2013).
18. S. Cinti, D. Talarico, G. Palleschi, D. Moscone and F. Arduini, *Analytica Chimica Acta*, **919**, 78 (2016).
19. S. P. Kounaves, Voltammetric techniques, in, p. 709, Prentice Hall, Upper Saddle River, NJ, USA (1997).
20. J. B. Allen and R. F. Larry, *Electrochemical methods fundamentals and applications*, John Wiley & Sons (2001).
21. C. Barus, I. Romanytsia, N. Striebig and V. Garçon, *Talanta*, **160**, 417 (2016).
22. D. R. Kumar, G. Dhakal, J. Lee, Y. R. Lee and J.-J. Shim, *Microchemical Journal*, **170**, 106639 (2021).
23. H. Wei, D. Pan, Z. Zhou, H. Han and R. Zhu, *Ecotoxicology and Environmental Safety*, **221**, 112444 (2021).
24. L. Guanghan, W. Xiaogang, L. Yanhua and Y. Shenlai, *Talanta*, **49**, 511 (1999).
25. J. Murphy and J. P. Riley, *Analytica Chimica Acta*, **27**, 31 (1962).
26. D. Hydes, M. Aoyama, A. Aminot, K. Bakker, S. Becker, S. Coverly, A. Daniel, A. Dickson, O. Grosso and R. Kerouel, (2010).
27. S. Motomizu and Z.-H. Li, *Talanta*, **66**, 332 (2005).
28. M. J. Moorcroft, J. Davis and R. G. Compton, *Talanta*, **54**, 785 (2001).

29. M. Pourbaix, *NACE*, **307** (1974).
30. K. Wang, Y.-S. Li and P. He, *Electrochimica acta*, **43**, 2459 (1998).
31. M. Bojinov, I. Betova and R. Raicheff, *Journal of Electroanalytical Chemistry*, **381**, 123 (1995).
32. M. N. Hull, *Journal of Electroanalytical Chemistry and Interfacial Electrochemistry*, **38**, 143 (1972).
33. V. S. Saji and C. W. Lee, *ChemSusChem*, **5**, 1146 (2012).
34. L. Guanghan, W. Xiaogang, L. Yanhua and Y. Shenlai, *Talanta*, **49**, 511 (1999).
35. W. F. Directive, *Journal reference OJL*, **327**, 1 (2000).
36. G. Ilangovan and K. Chandrasekara Pillai, *Langmuir*, **13**, 566 (1997).
37. J. Jońca, C. Barus, W. Giraud, D. Thouron, V. Garçon and M. Comtat, *Int. J. Electrochem. Sci*, **7**, 7325 (2012).
38. C. Rong and F. C. Anson, *Inorganica chimica acta*, **242**, 11 (1996).
39. A. V. Kolliopoulos, D. K. Kampouris and C. E. Banks, *Analytical chemistry*, **87**, 4269 (2015).
40. M. I. Prodromidis, *Electrochimica Acta*, **55**, 4227 (2010).
41. B. A. Boukamp, *Solid state ionics*, **20**, 31 (1986).
42. M. Dijksma, B. A. Boukamp, B. Kamp and W. Van Bennekom, *Langmuir*, **18**, 3105 (2002).
43. Y. Bai, J. Tong, J. Wang, C. Bian and S. Xia, *IET nanobiotechnology*, **8**, 31 (2014).
44. S.-H. Choi and J.-W. Kim, *Bulletin of the Korean Chemical Society*, **30**, 810 (2009).
45. B. Wang and S. Dong, *Electrochimica acta*, **41**, 895 (1996).
46. G. L. Long and J. D. Winefordner, *Analytical chemistry*, **55**, 712A (1983).
47. Y. Huang, *International Journal of Electrochemical Science*, 4677 (2017).
48. H. Satoh, Y. Miyazaki, S. Taniuchi, M. Oshiki, R. M. L. D. Rathnayake, M. Takahashi and S. Okabe, *Analytical Sciences*, **33**, 825 (2017).
49. C. Topcu, B. Caglar, A. Onder, F. Coldur, S. Caglar, E. K. Guner, O. Cubuk and A. Tabak, *Materials Research Bulletin*, **98**, 288 (2018).
50. L. Li, G. Shang and W. Qin, *Analyst*, **141**, 4573 (2016).
51. D. Talarico, F. Arduini, A. Amine, D. Moscone and G. Palleschi, *Talanta*, **141**, 267 (2015).
52. E. Ogabiela, S. B. Adeloju, J. Cui, Y. Wu and W. Chen, *Biosens Bioelectron*, **71**, 278 (2015).

53. J. Cui, E. E. Ogabiela, J. Hui, Y. Wang, Y. Zhang, L. Tong, J. Zhang, S. B. Adeloju, X. Zhang and Y. Wu, *Journal of The Electrochemical Society*, **162**, B62 (2014).
54. S. S. Shankar, B. K. Swamy and B. Chandrashekar, *Journal of Molecular Liquids*, **168**, 80 (2012).
55. M. Kowalcze and M. Jakubowska, *Analytical biochemistry*, **543**, 12 (2018).
56. B. Cosović and V. Vojvodić, *Limnology and Oceanography*, **27**, 361 (1982).
57. J.-Z. Zhang, C. J. Fischer and P. B. Ortner, *Talanta*, **49**, 293 (1999).
58. L. Otto, J. Zimmerman, G. Furnes, M. Mork, R. Saetre and G. Becker, *Netherlands journal of sea research*, **26**, 161 (1990).
59. R. Reuter, T. H. Badewien, A. Bartholomä, A. Braun, A. Lübben and J. Rullkötter, *Ocean Dynamics*, **59**, 195 (2009).
60. M. Carstens, U. Claussen, M. Bergemann and T. Gaumert, *Aquatic Conservation: Marine and Freshwater Ecosystems*, **14**, S81 (2004).
61. M. Simon, V. Bekele, V. Kulasova, C. Maul, R. Oppermann and P. Rehak, *Internationale Kommission zum Schutz der Elbe, Magdeburg* (2005).
62. M. J. Boehlich and T. Strotmann, *Die Küste, 87-Online First* (2019).
63. M. Bergemann and T. Gaumert, *FGG Elbe, Hamburg* (2010).
64. T. Pohlmann, *Continental Shelf Research*, **26**, 2367 (2006).
65. M. Grunwald, O. Dellwig, C. Kohlmeier, N. Kowalski, M. Beck, T. H. Badewien, S. Kotzur, G. Liebezeit and H.-J. Brumsack, *Journal of Sea Research*, **64**, 199 (2010).
66. A. Williams, D. Tudor and M. Gregory, Marine debris—onshore, offshore, seafloor litter. Encylopedia of Coastal Science (Encyclopedia of Earth Sciences Series), in, Berlin, Germany: Springer (2005).
67. H. Heyen and J. W. Dippner, *Tellus A*, **50**, 545 (1998).
68. R. Schlitzer, Ocean Data View, ODV 5.2. 1, in (2020). https://odv.awi.de.

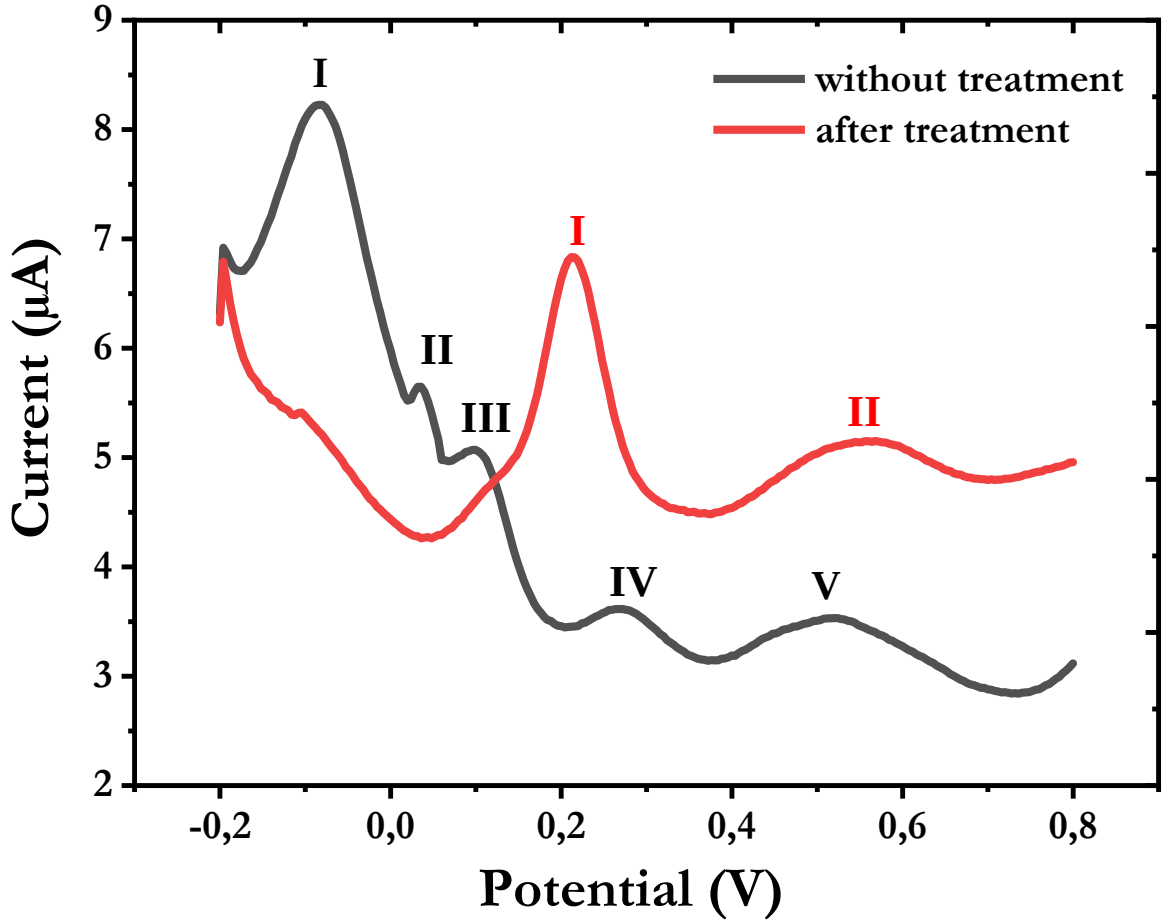

Figure 1. Comparison between square wave voltammograms of the pretreated (red line) and the untreated (black line) molybdate / CPE in a solution of 35 g/L NaCl (pH 0.8) containing 0.5 µM PO_4^{3-} with square wave frequency 150 Hz, 50 mV square wave amplitude, 1 mV step potential and 75 s quiet time. The pretreatment was performed by CV for 10 scanning cycles in 0.1 M NaOH from - 0.5 V to 0.5 V at a scan rate of 0.1 V/s.

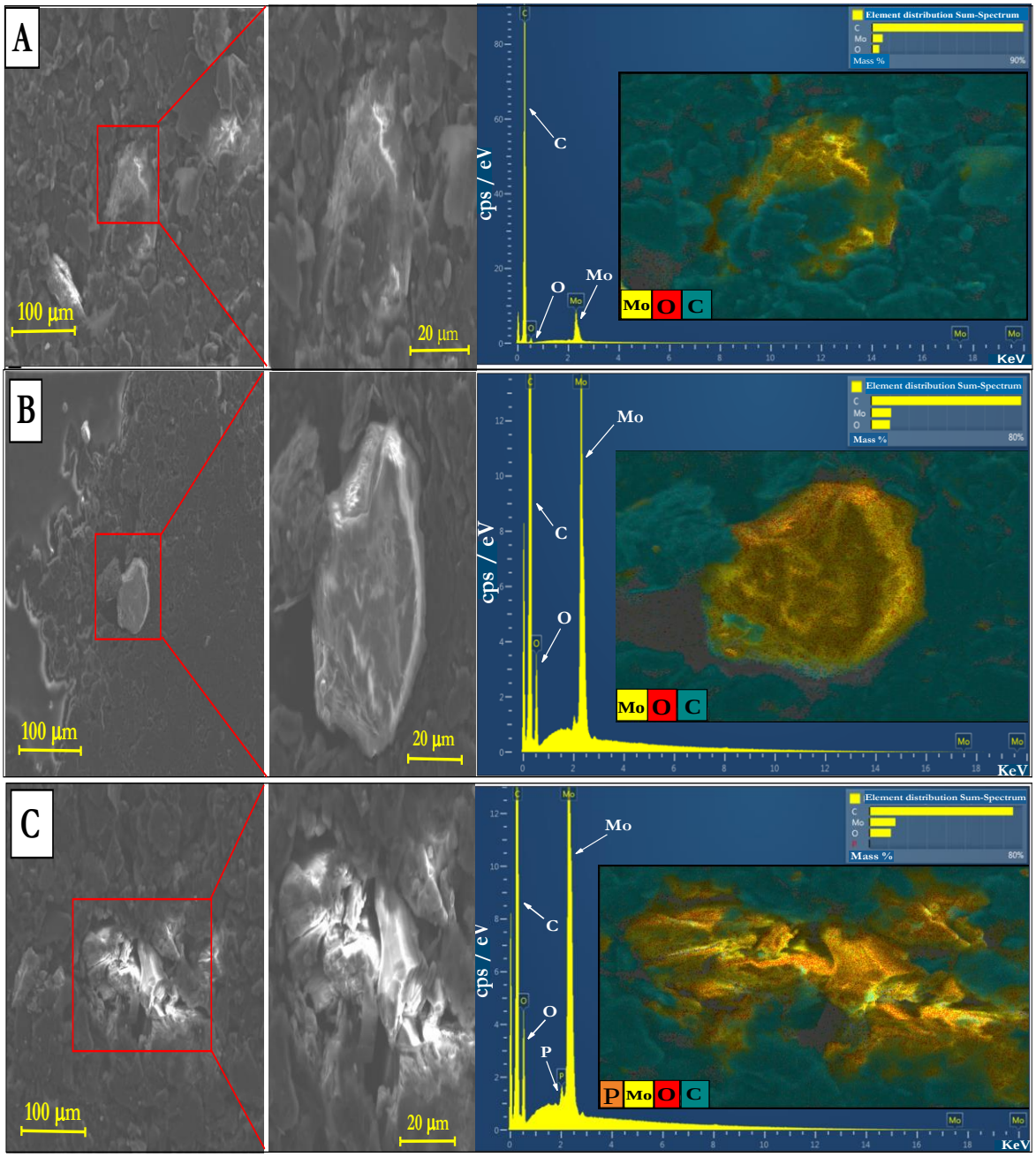

Figure 2. Field emission-scanning electron microscope images with different magnifications, energy dispersive x-ray spectrum and elemental mapping analysis showing the distribution of C, Mo, O and P for (A) molybdate / CPE without modification, (B) after CV of molybdate / CPE in 0.1 M NaOH and (C) after SWV of molybdate / CPE in a solution of 30 g/L NaCl (pH 0.8) with 1 M PO_4^{3-}.

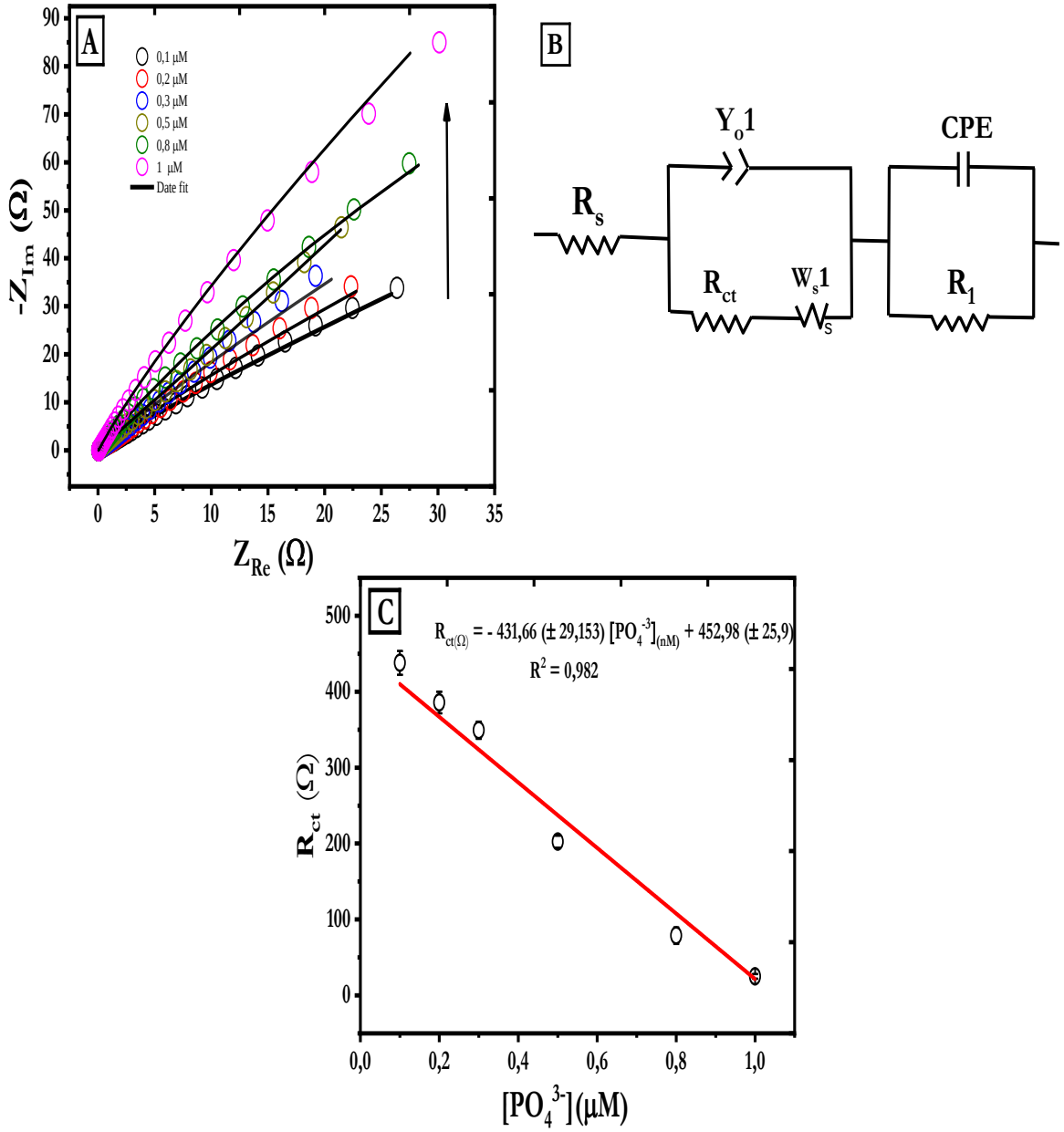

Figure 3. (A) Nyquist plots (Z(real) vs. −Z(imaginary)) obtained for molybdate/CPE for 0.1, 0.2, 0.3, 0.5, 0.8, and 1 µM PO_4^{3-}, each in 35-g/L NaCl solution (pH 0.8). The circles denote the experimental data, whereas the solid lines represent the data measured using the modified Randles equivalent circuit in (B) used to fit the experimental data to extrapolate impedance parameters. (C) The calibration curve for various PO_4^{3-} concentrations at the charge-transfer resistance (R_{ct}). The data points are expressed as a mean ± SD of three replicated measurements, and the fitted curve represents the linear regression.

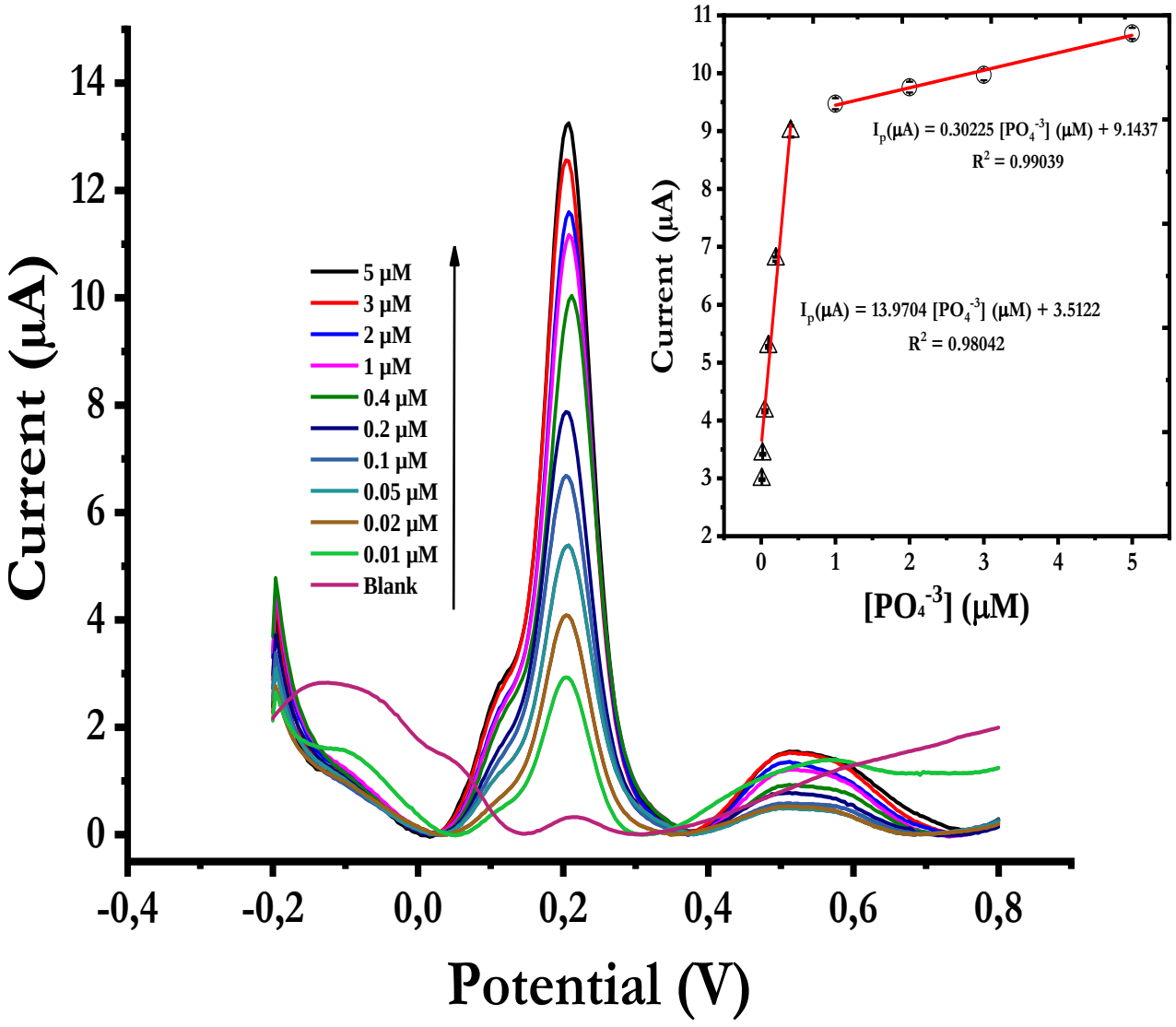

Figure 4. Square wave voltammograms of different PO_4^{3-} concentrations (0.01, 0.02, 0.05, 0.1, 0.2, 0.4, 1, 2, 3, and 5 µM) on molybdate/CPE in 35 g/L NaCl (pH 0.8), frequency of 150 Hz, and amplitude of 50 mV, with the calibration curve shown in the inset that is related to the regression equations and R^2 value. (**Error bar *n* = 5**).

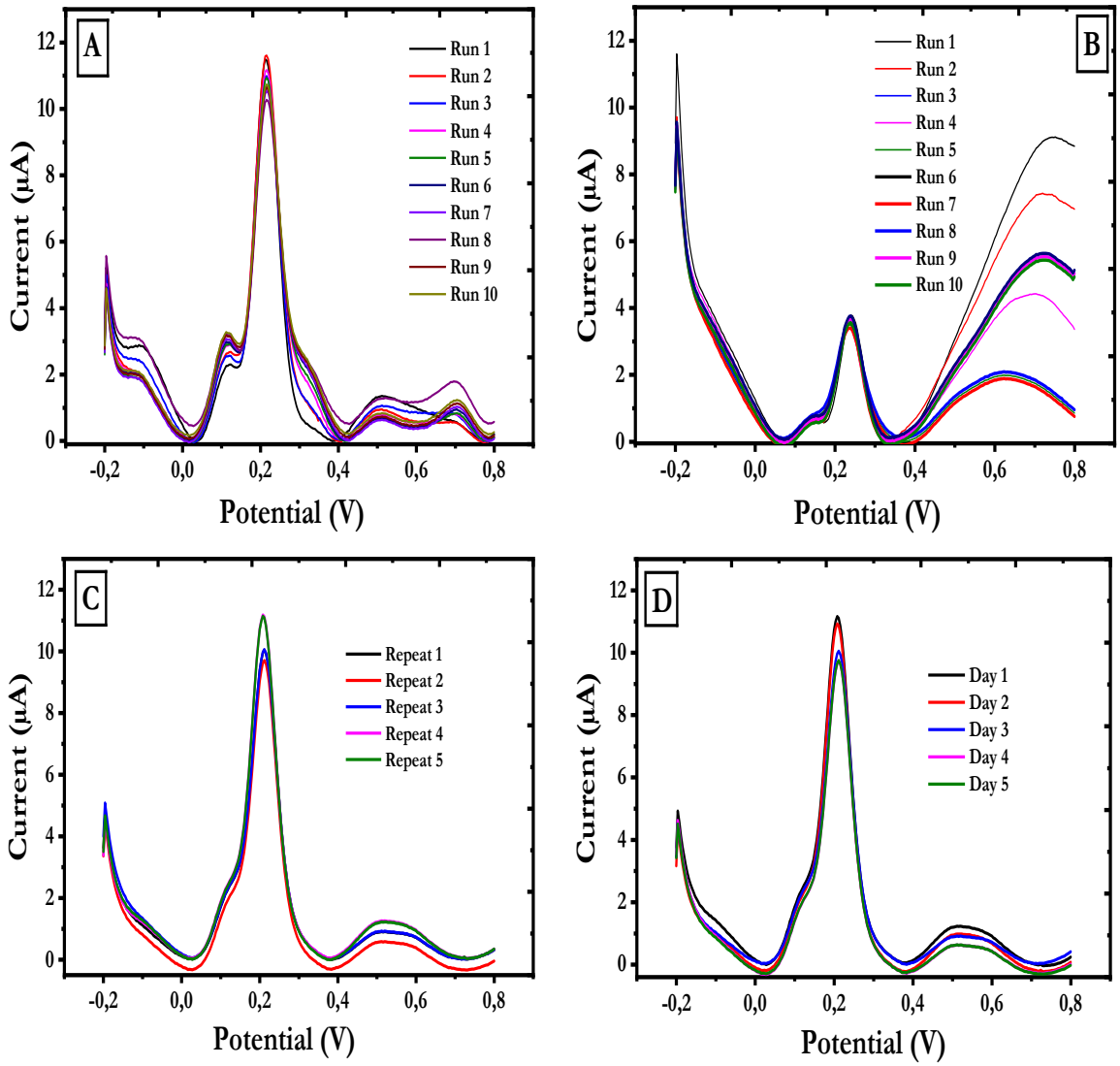

Figure 5. Repeatability of molybdate/CPE sensor toward PO_4^{3-}detection. (A) Square-wave voltammograms of 5 µM PO_4^{3-}, (B) square-wave voltammograms of 0.2 µM PO_4^{3-} in 30-g/L NaCl, pH 0.8. Ten repetitive measurements were reordered at every 100 intervals over 20 min with 10 scanning cyclic voltammograms into 0.1-M NaOH after each measurement. (C) Reproducibility of molybdate/CPE to 5 µM PO_4^{3-} into artificial seawater (pH 0.8) with five fabricated electrodes. (D) Operative stability to 5 µM PO_4^{3-} into artificial seawater with stored molybdate/CPE (at room temperature) over five days. The SWV potential ranges from −0.2 V to 0.8 V (vs. Ag–AgCl) using a 150 Hz frequency, an amplitude of 50 mV, and step potential of 1 mV.

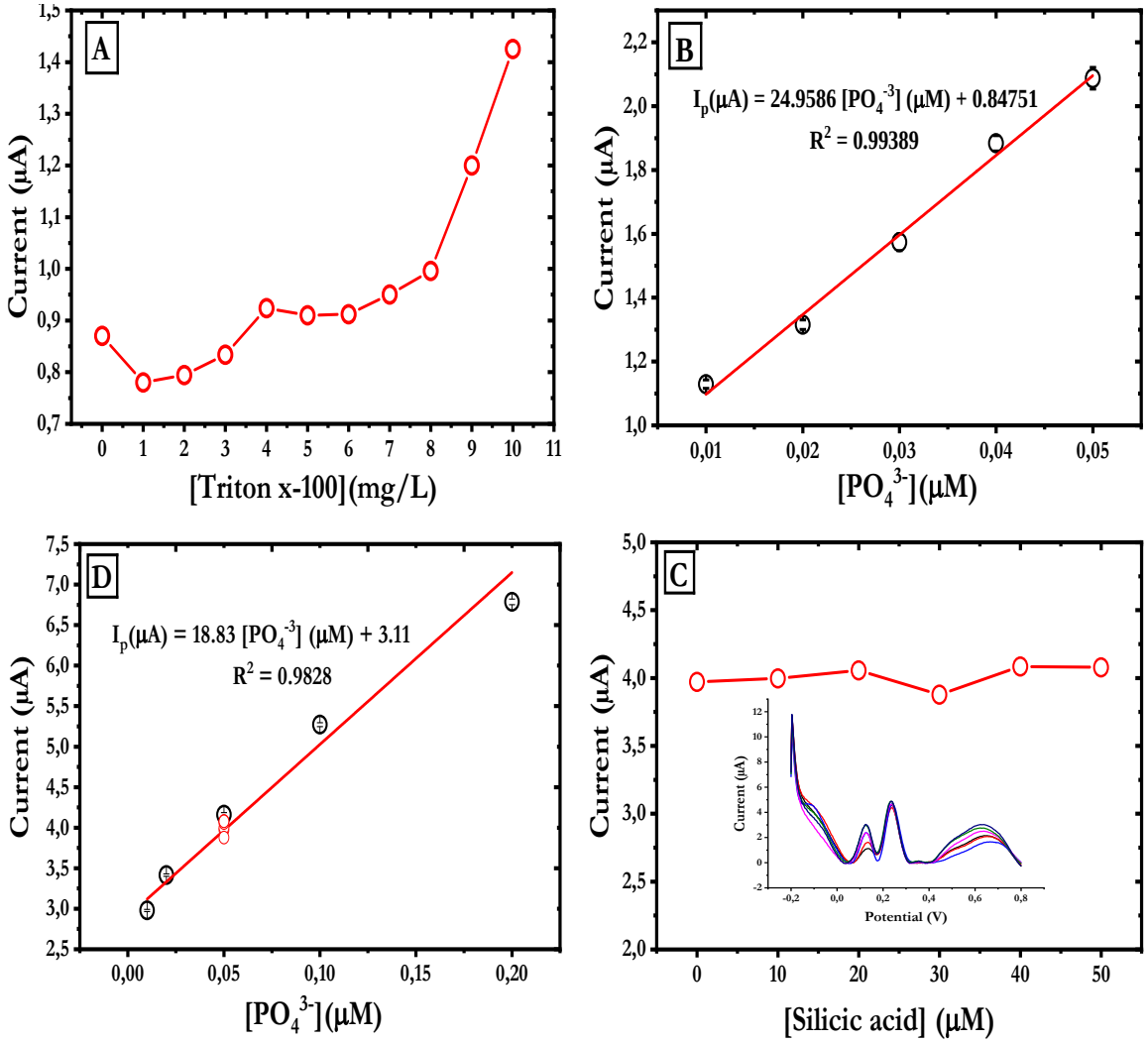

Figure 6. Interference effect from A) the nonionic surfactant Triton X-100 on the peak current of 0.01 µM PO_4^{3-} in 30 g/L NaCl (pH 0.8). B) Calibration curve constructed from 0.01, 0.02, 0.03, 0.04, and 0.05 µM PO_4^{3-} containing 10 ppm of Triton X-100 with the related regression equation and R^2. C) The interference study of silicic acid at concentrations of 0, 10, 20, 30, 40, and 50 µM in a solution containing 0.05 µM PO_4^{3-} in artificial sea water. mD) Calibration curve from SWVs at PO_4^{3-} concentrations of 0.01, 0.02, 0.05, 0.1, 0.2 µM at the peak at 0.2 V, including the peak current of 0.05 µM PO_4^{3-} containing different concentrations of silicic acid.

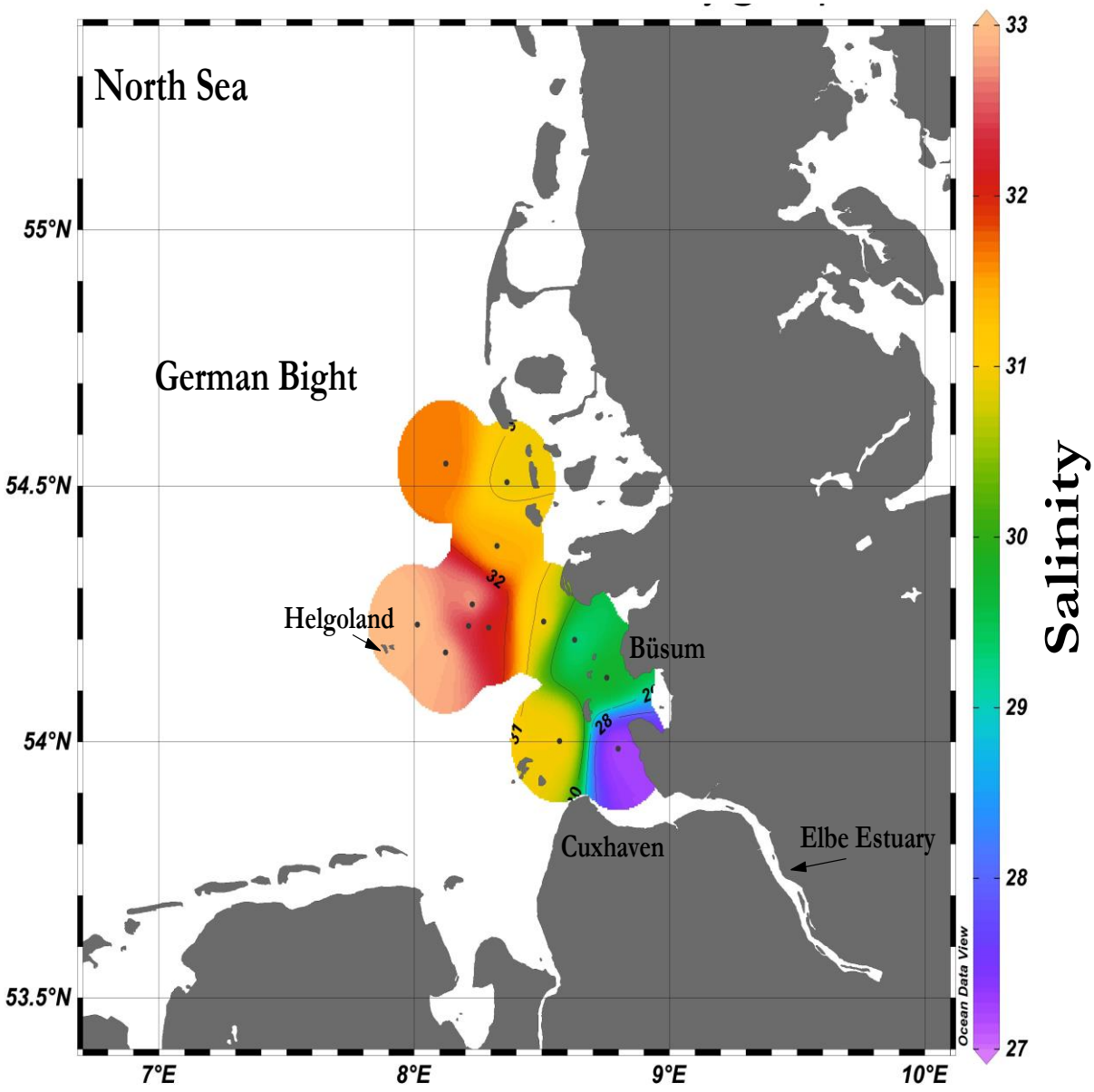

Figure 7. Overview of the sampling stations (red dots) in the German Bight (North Sea) at the outflow of the Elbe River. Locations of Helgoland Island and Elbe Estuary are denoted on the map. The map showed the regional overview of the study area reflecting the spatial distribution of seawater salinity. Map plotted using ODV 5.3.0 (68).

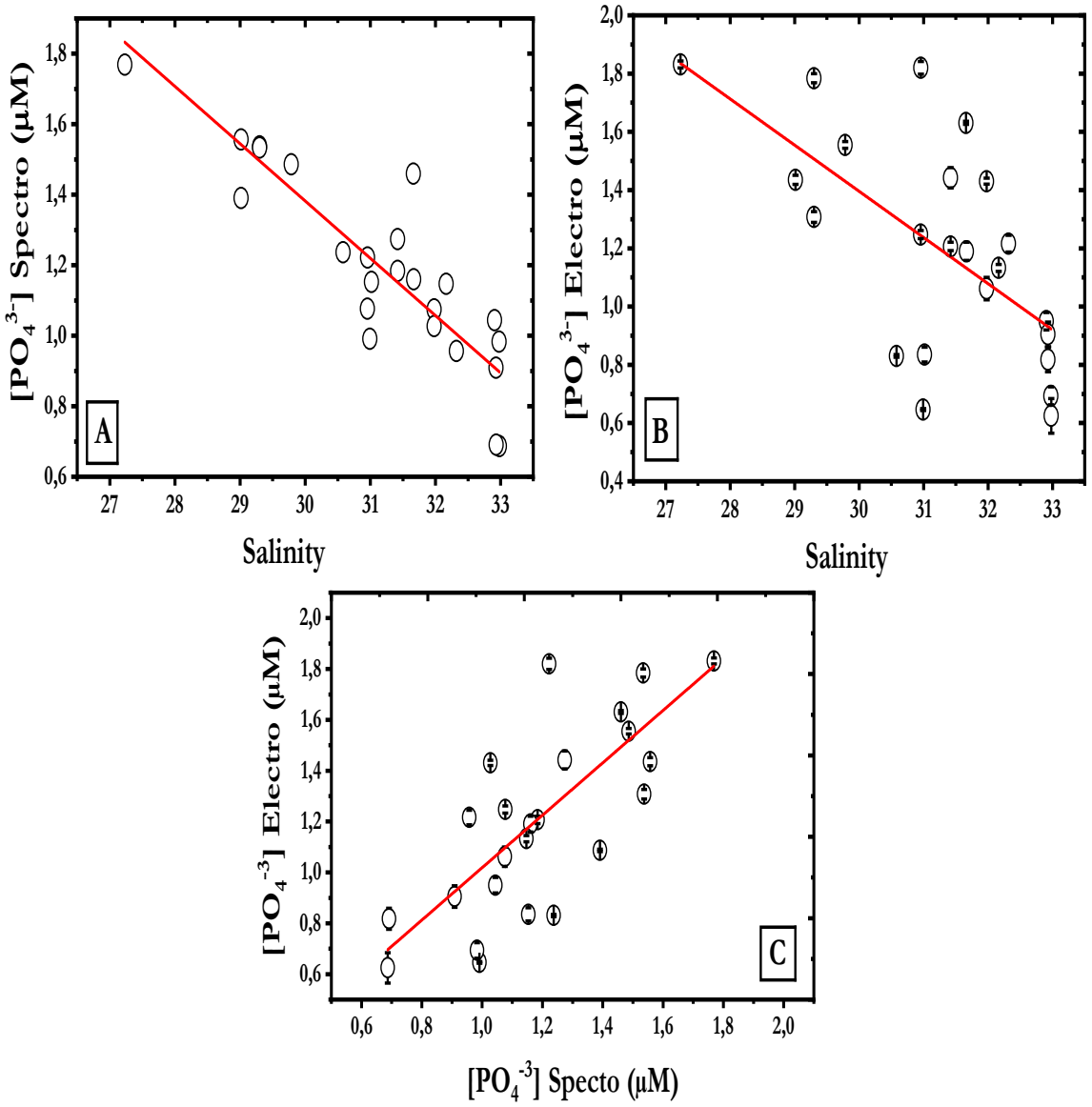

Figure 8. Property to property plots for the discrete samples collected. (A) PO_4^{3-} measured using the classical colorimetric method vs. salinity during CTD casts $y = -0.16259x + 6.259$, $R^2 = 0.78129$. (B) PO_4^{3-} measured electrochemically vs. salinity during CTD casts $y = -0.1586x + 6.1539$, $R^2 = 0.4018$. (C) PO_4^{3-} measured using the colorimetric method vs. PO_4^{3-} measured electrochemically $y = 1.573x - 0.8446$, $R^2 = 0.6812$.

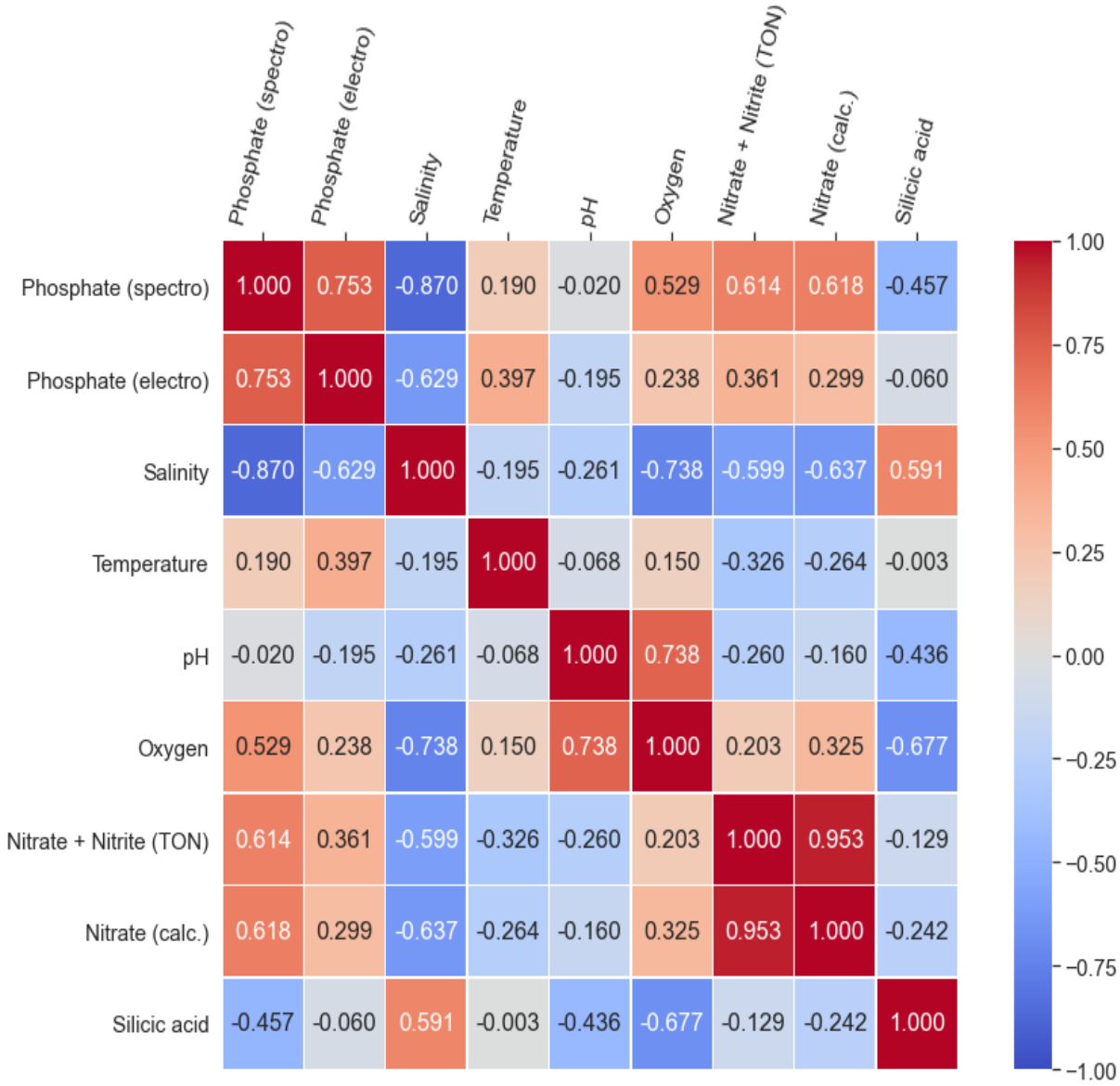

Figure 9. Spearman correlation matrix of different variables for the discrete samples collected off the North Sea. Positive correlation coefficients are shown in red boxes and negative correlation coefficients in blue boxes ($p < 0.01$).